Supporting Information

Efficient Asymmetric Synthesis of Ethyl (*S*)-4-Chloro-3-hydroxybutyrate Using Alcohol Dehydrogenase *Sm*ADH31 with High Tolerance of Substrate and Product in a Monophasic Aqueous System

Zeyu Yang[1], Wenjie Ye[1], Youyu Xie[1], Qinghai Liu[1], Rong Chen[2], Hualei Wang[1,*] and Dongzhi Wei[1]

[1]State Key Laboratory of Bioreactor Engineering, New World Institute of Biotechnology, East China University of Science and Technology, Shanghai 200237, PR China

[2]School of Medicine, Hangzhou Normal University, Hangzhou 311121, PR China

*Corresponding author:

Hualei Wang: hlwang@ecust.edu.cn

Table S1. Primers information of *Sm*ADHs and *Ar*ADHs in ADHs library.

Entry	Enzyme	Accession number	Function	Sequence	
1-30	*Sm*ADH1-30	Refer to our previous work.[1]			
31	*Sm*ADH31	WP_032130254.1	Putative acetoacetyl-CoA reductase	forward	5′-CGC**GGATCC**ATGACATCTCGCGTCGCAC-3′
				reverse	5′-CCC**AAGCTT**TTACCAACCCATATGGTGGC-3′
32	*Sm*ADH32	WP_057500466.1	Alcohol dehydrogenase protein	forward	5′-GGAATTC**CATATG**ACCCTCTCCCCCACCC-3′
				reverse	5′-CGC**GGATCC**TCAAGGCCGCAGCAGCAC-3′
33	*Sm*ADH33	WP_057502264.1	Alcohol dehydrogenase	forward	5′-GGAATTC**CATATG**AATTCGACCATGAAGGCC-3′
				reverse	5′-CGC**GGATCC**TCAGGCGGCGAAGTCGAG-3′
34	*Ar*ADH1	WP_005017515.1	Zinc-type alcohol dehydrogenase	forward	5′-GGAATTC**CATATG**CGCGCTCTTACATATCATG-3′
				reverse	5′-CGC**GGATCC**TTAAGGAGTAAGGATTACCTTACGACA-3′
35	*Ar*ADH2	WP_005405891.1	Cinnamic acid-dihydrodiol reductase	forward	5′-GGAATTC**CATATG**GGTTGGCTAAAAGGTGAAG-3′
				reverse	5′-CGC**GGATCC**TTATTCATCGAAGAAGCCTGCA-3′
36	*Ar*ADH3	WP_005406939.1	Dehydrogenase SDR family protein	forward	5′-CGC**GGATCC**ATGGCAAGTCCGCAATTAAATA-3′
				reverse	5′-CCC**AAGCTT**TCACTTTACTTTCATTTTACGGATCA-3′
37	*Ar*ADH4	WP_005015831.1	Alcohol dehydrogenase	forward	5′-GGAATTC**CATATG**GCTAAACCTTATTATGAATTTTTC-3′
				reverse	5′-CGC**GGATCC**TTACCAAGCCTTTTGTAAAATCGC-3′
38	*Ar*ADH5	WP_005405626.1	(*R,R*)-butanediol dehydrogenase	forward	5′-GGAATTC**CATATG**AAAGCAGCTCGTTTTTATGATA-3′
				reverse	5′-CGC**GGATCC**TTAGGGATGGACAATAATTTTAACAGC-3′
39	*Ar*ADH6	WP_005406490.1	Alcohol dehydrogenase	forward	5′-CGC**GGATCC**ATGGGCCAATTTCAGTTTCAAAC-3′
				reverse	5′-CCC**AAGCTT**TCATGAATAAATGGCTCGATATATATTG-3′
40	*Ar*ADH7	WP_005019926.1	Probable alcohol dehydrogenase	forward	5′-GGAATTC**CATATG**GCTTTTAAAAATATTGCAGATC-3′
				reverse	5′-CGC**GGATCC**TTACATCGCCGCTTTAAACATT-3′
41	*Ar*ADH8	WP_005027729.1	Histidinol dehydrogenase	forward	5′-GGAATTC**CATATG**CGACGTTTATCGACTCAAG-3′
				reverse	5′-CGC**GGATCC**TCAATAGCGATAGCGGGCTG-3′
42	*Ar*ADH9	WP_005407224.1	Zinc-type ADH-like protein	forward	5′-CCG**GAATTC**ATGAGTCAGAAGAATACTATTCGTGCC-3′
				reverse	5′-CCC**AAGCTT**TTAGTCAAAATCTGCTTTTAAAACCACC-3′

Table S2. Screening and coenzyme dependence of *Sm*ADHs and *Ar*ADHs.

Entry	Enzyme	Coenzyme dependence	Relative activity (%) [a]	*ee* (%)
1	*Sm*ADH1	-	nd.[b]	nd.
2	*Sm*ADH2	NADH	78	>99.9 (*S*)
3	*Sm*ADH3	-	nd.	nd.
4	*Sm*ADH4	-	nd.	nd.
5	*Sm*ADH5	NADPH	34	96.4 (*S*)
6	*Sm*ADH6	-	nd.	nd.
7	*Sm*ADH7	-	nd.	nd.
8	*Sm*ADH8	-	nd.	nd.
9	*Sm*ADH9	-	nd.	nd.
10	*Sm*ADH10	-	nd.	nd.
11	*Sm*ADH11	NADPH	13	93.2 (*R*)
12	*Sm*ADH12	-	nd.	nd.
13	*Sm*ADH13	NADPH	33	98.6 (*S*)
14	*Sm*ADH14	-	nd.	nd.
15	*Sm*ADH15	-	nd.	nd.
16	*Sm*ADH16	-	nd.	nd.
17	*Sm*ADH17	-	nd.	nd.
18	*Sm*ADH18	NADH	16	79.9 (*S*)
19	*Sm*ADH19	-	nd.	nd.
20	*Sm*ADH20	-	nd.	nd.
21	*Sm*ADH21	NADH	22	>99.9 (*S*)
22	*Sm*ADH22	-	nd.	nd.
23	*Sm*ADH23	-	nd.	nd.
24	*Sm*ADH24	-	nd.	nd.
25	*Sm*ADH25	-	nd.	nd.
26	*Sm*ADH26	-	nd.	nd.
27	*Sm*ADH27	-	nd.	nd.
28	*Sm*ADH28	NADH	8	>99.9 (*S*)
29	*Sm*ADH29	-	nd.	nd.
30	*Sm*ADH30	-	nd.	nd.
31	*Sm*ADH31	NADPH	100	>99.9 (*S*)
32	*Sm*ADH32	-	nd.	nd.
33	*Sm*ADH33	-	nd.	nd.
34	*Ar*ADH1	-	nd.	nd.
35	*Ar*ADH2	-	nd.	nd.
36	*Ar*ADH3	NADPH	15	99.6 (*S*)
37	*Ar*ADH4	-	nd.	nd.
38	*Ar*ADH5	-	nd.	nd.
39	*Ar*ADH6	-	nd.	nd.
40	*Ar*ADH7	-	nd.	nd.
41	*Ar*ADH8	-	nd.	nd.
42	*Ar*ADH9	-	nd.	nd.

[a] Relative activity was measured using crude *Ar*ADHs and *Sm*ADHs under standard conditions. The relative activity of *Sm*ADH31 was defined as 100% and other ADHs were expressed as a percentage of *Sm*ADH31 activity.

[b] Not detected.

Table S3. Kinetic parameters for reduction of **5a**, **6a**, **7a**, **10a**, **11a** and **24a** by *Sm*ADH31.

Enzyme	Substrate	K_m (mM)	k_{cat} (s^{-1})	k_{cat}/K_m ($mM^{-1}\ s^{-1}$)
*Sm*ADH31	**5a**	1.2	142	1.2×10^2
*Sm*ADH31	**6a**	0.73	190	2.6×10^2
*Sm*ADH31	**7a**	0.67	194	2.9×10^2
*Sm*ADH31	**10a**	0.42	232	5.5×10^2
*Sm*ADH31	**11a**	0.84	151	1.8×10^2
*Sm*ADH31	**24a**	2.5	74	29.6

Table S4. Asymmetric transformation of COBE using lyophilized *E. coli* cells coexpressing *Sm*ADH31 and GDH.

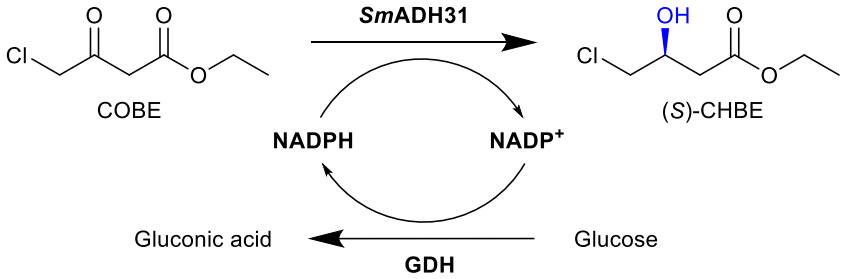

Entry	Ketone		NADP+	Cell	Time	Conv.	*ee*	Yield
	($g\ L^{-1}$)	(M)	(mM) [a]	($g\ L^{-1}$)	(h)	(%) [b]	(%) [b]	(%)
1	660	4	0.4	30	3	>99.9	*S* (>99.9)	92
2	660	4	0.3	20	4	>99.9	*S* (>99.9)	92
3	660	4	0.1	20	5	>99.9	*S* (>99.9)	92
5	660	4	0	20	6	>99.9	*S* (>99.9)	92

[a] The values represent the concentration of exogenous $NADP^+$.
[b] Conversion and *ee* values were detected by GC instrument (Table S5).

Table S5. HPLC and GC analytic methods for chiral alcohols.

Product	Chiral column	Conditions
(*R,S*)-**1b**	CP-Chirasil-Dex CB (25 m×0.32 mm, 0.25 μm, Agilent, USA)	70 °C; Inc./dec. 250 °C; flow rate: 0.7 ml min^{-1}; nitrogen
(*R,S*)-**2b**	CP-Chirasil-Dex CB (25 m×0.32 mm, 0.25 μm, Agilent, USA)	70 °C; Inc./dec. 250 °C; flow rate: 0.7 ml min^{-1}; nitrogen
(*R,S*)-**3b**	CP-Chirasil-Dex CB (25 m×0.32 mm, 0.25 μm, Agilent, USA)	80 °C; Inc./dec. 250 °C; flow rate: 0.8 ml min^{-1}; nitrogen
(*R,S*)-**4b**	CP-Chirasil-Dex CB (25 m×0.32 mm, 0.25 μm, Agilent, USA)	160 °C; Inc./dec. 250 °C; flow rate: 0.8 ml min^{-1}; nitrogen
(*R,S*)-**5b**	CP-Chirasil-Dex CB (25 m×0.32 mm, 0.25 μm, Agilent, USA)	90 °C 3 min, 10 °C min^{-1}, 160 °C; Inc./dec. 250 °C; 1.0 ml min^{-1}; nitrogen
(*R,S*)-**6b**	CP-Chirasil-Dex CB (25 m×0.32 mm, 0.25 μm, Agilent, USA)	80 °C; Inc./dec. 250 °C; flow rate: 0.6 ml min^{-1}; nitrogen
(*R,S*)-**7b**	CP-Chirasil-Dex CB (25 m×0.32 mm, 0.25 μm, Agilent, USA)	80 °C; Inc./dec. 250 °C; flow rate: 0.6 ml min^{-1}; nitrogen
(*R,S*)-**8b**	CP-Chirasil-Dex CB (25 m×0.32 mm, 0.25 μm, Agilent, USA)	90 °C; Inc./dec. 250 °C; flow rate: 0.8 ml min^{-1}; nitrogen
(*R,S*)-**9b**	CP-Chirasil-Dex CB (25 m×0.32 mm, 0.25 μm, Agilent, USA)	90 °C 2 min, 5 °C min^{-1}, 160 °C; Inc./dec. 250 °C; 1.0 ml min^{-1}; nitrogen
(*R,S*)-**10b**	CP-Chirasil-Dex CB (25 m×0.32 mm, 0.25 μm, Agilent, USA)	90 °C 2 min, 5 °C min^{-1}, 160 °C; Inc./dec. 250 °C; 1.0 ml min^{-1}; nitrogen
(*R,S*)-**11b**	CP-Chirasil-Dex CB (25 m×0.32 mm, 0.25 μm, Agilent, USA)	80 °C; Inc./dec. 250 °C; flow rate: 0.6 ml min^{-1}; nitrogen
(*R,S*)-**12b**	CP-Chirasil-Dex CB (25 m×0.32 mm, 0.25 μm, Agilent, USA)	90 °C; Inc./dec. 250 °C; flow rate: 0.7 ml min^{-1}; nitrogen
(*R,S*)-**13b**	Beta DEX™ 120 (30 m×0.25 mm, 0.25 μm, Supelco, USA)	130 °C; Inc./dec. 280 °C; flow rate: 0.8 ml min^{-1}; nitrogen
(*R,S*)-**14b**	Chiralcel OD-H column (0.46 mm×250 mm, 5 μm, Diacel, Japan)	hexane/2-propanol (95:5, v/v); flow rate: 1 mL min^{-1}; 210 nm
(*R,S*)-**15b**	Chiralcel OB-H column (0.46 mm×250 mm, 5 μm, Diacel, Japan)	hexane/2-propanol (95:5, v/v); flow rate: 1 mL min^{-1}; 210 nm
(*R,S*)-**16b**	Chiralcel OD-H column (0.46 mm×250 mm, 5 μm, Diacel, Japan)	hexane/2-propanol (95:5, v/v); flow rate: 1 mL min^{-1}; 210 nm
(*R,S*)-**17b**	Beta DEX™ 120 (30 m×0.25 mm, 0.25 μm, Supelco, USA)	140 °C; Inc./dec. 280 °C; flow rate: 0.8 ml min^{-1}; nitrogen
(*R,S*)-**18b**	Beta DEX™ 120 (30 m×0.25 mm, 0.25 μm, Supelco, USA)	150 °C; Inc./dec. 280 °C; flow rate: 0.8 ml min^{-1}; nitrogen
(*R,S*)-**19b**	Beta DEX™ 120 (30 m×0.25 mm, 0.25 μm, Supelco, USA)	160 °C; Inc./dec. 280 °C; flow rate: 0.8 ml min^{-1}; nitrogen
(*R,S*)-**20b**	Beta DEX™ 120 (30 m×0.25 mm, 0.25 μm, Supelco, USA)	170 °C; Inc./dec. 280 °C; flow rate: 0.8 ml min^{-1}; nitrogen
(*R,S*)-**21b**	Beta DEX™ 120 (30 m×0.25 mm, 0.25 μm, Supelco, USA)	150 °C; Inc./dec. 280 °C; flow rate: 0.7 ml min^{-1}; nitrogen
(*R,S*)-**22b**	CP-Chirasil-Dex CB (25 m×0.32 mm, 0.26 μm, Agilent, USA)	140 °C; Inc./dec. 250 °C; flow rate: 0.6 ml min^{-1}; nitrogen
(*R,S*)-**23b**	CP-Chirasil-Dex CB (25 m×0.32 mm, 0.26 μm, Agilent, USA)	130 ℃; Inc./dec. 250℃; flow rate: 0.6 ml min^{-1}; nitrogen
(*R,S*)-**24b**	Chiralcel OB-H column (0.46 mm×250 mm, 5 μm, Diacel, Japan)	hexane/2-propanol (95:5, v/v); flow rate: 1.0 mL min^{-1}; 254 nm

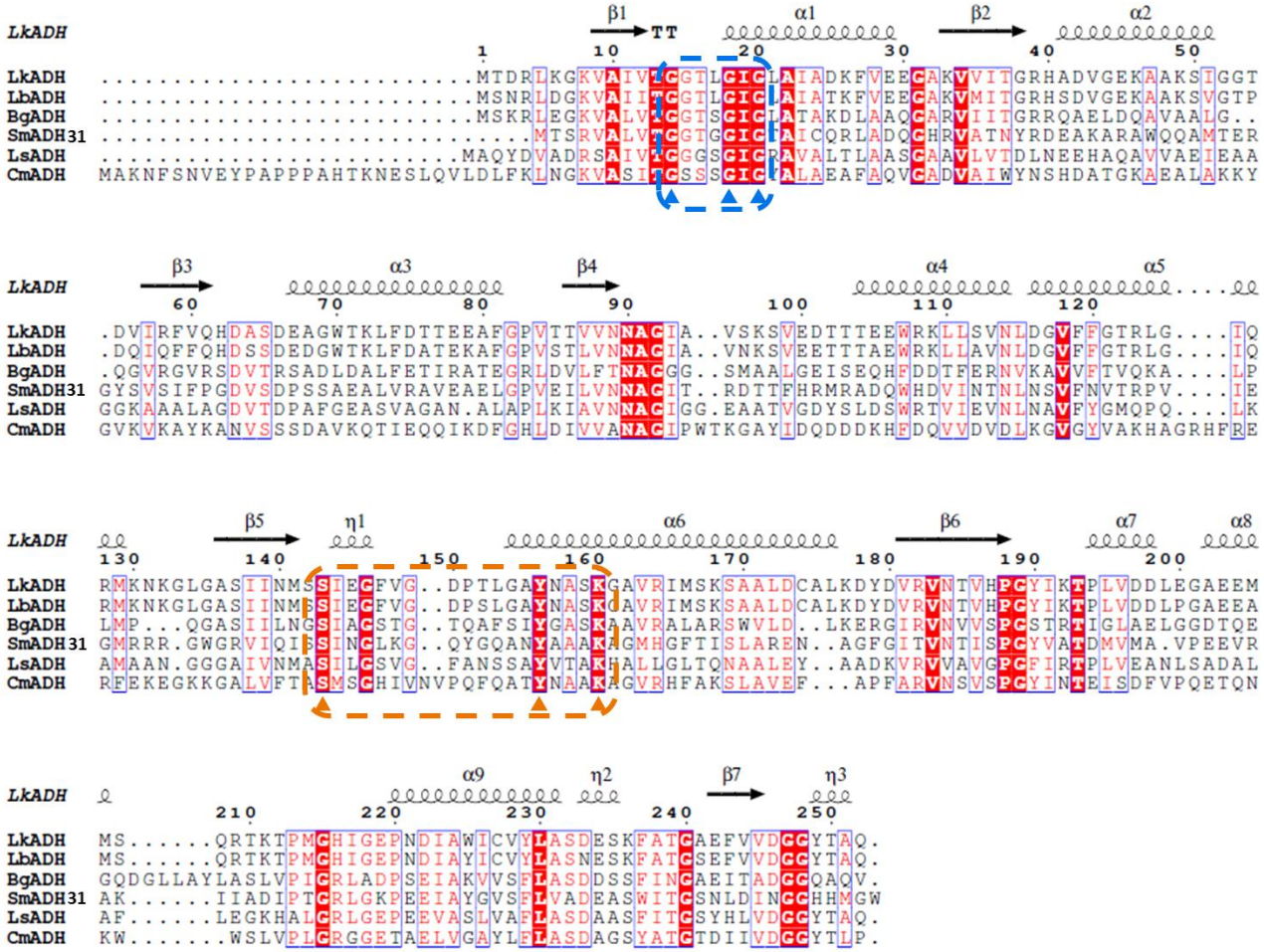

Figure S1. Sequence alignment of *Sm*ADH31 and other ADHs containing *Lk*ADH, *Lb*ADH, *Bg*ADH, *Ls*ADH and *Cm*ADH. Blue triangles represent the conserved area of the coenzyme binding motif. Orange triangles represent the conserved residues of the catalytic triads.

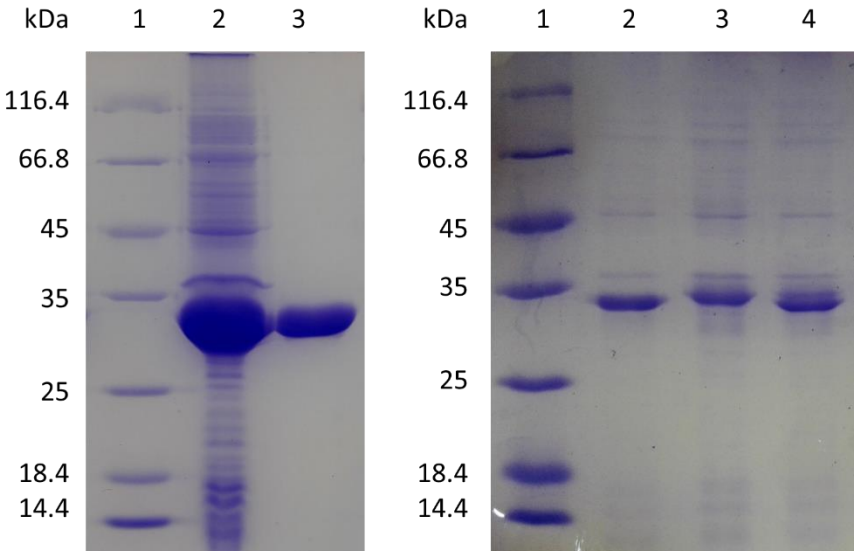

Figure S2. SDS-PAGE analysis of crude *Sm*ADH31, GDH, co-expressed proteins and purified *Sm*ADH31. (A) Lane 1, standard protein marker. Lane 2, crude *Sm*ADH31 extract. Lane 3, purified *Sm*ADH31. (B) Lane 1, standard protein marker. Lane 2, crude *Sm*ADH31 extract. Lane 3, crude GDH extract. Lane 4, crude coexpressed protein extracts containing *Sm*ADH31 and GDH.

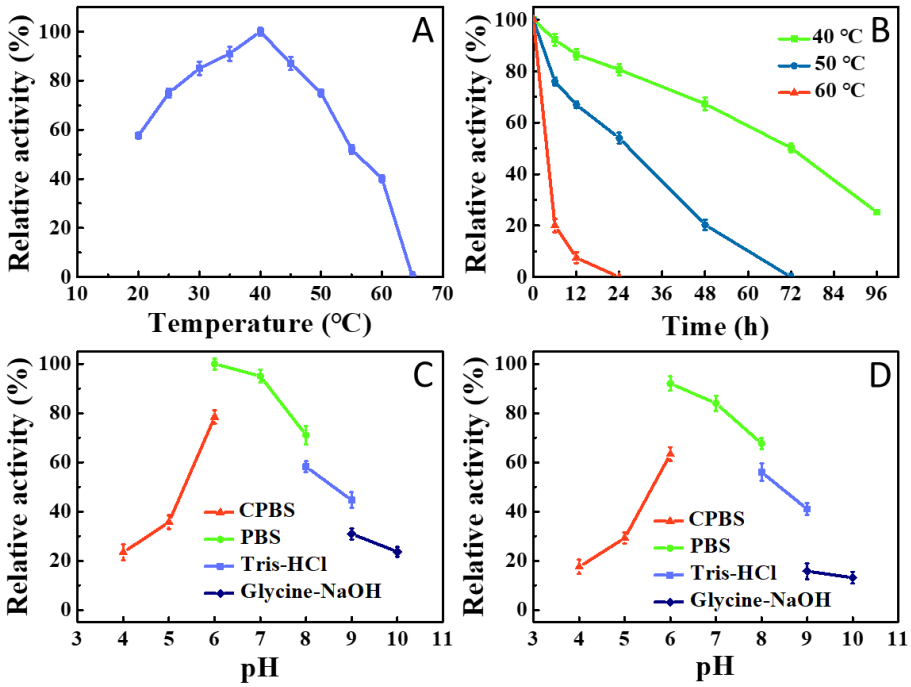

Figure S3. Effects of temperature and pH on the enzymatic activity of *Sm*ADH31. All tests were performed under standard conditions. (A) Temperature-activity curve of *Sm*ADH31 from 20 °C to 65 °C; (B) Thermal stability was evaluated by incubating the purified *Sm*ADH31 at 40 °C, 50 °C and 60 °C for 96 h; (C) Optimum pH was determined in 50 mM of the following buffers: pH 4.0-6.0 sodium citrate, pH 6.0-8.0 sodium phosfate buffer, pH 8.0-9.0 Tris (hydroxymethyl) aminomethane-HCl and pH 9.0-10.0 glycine-NaOH; (D) pH stability was evaluated by incubating the purified *Sm*ADH31 in the above buffers at 4 °C for 24 h. The activity of the enzyme without incubation was defined as 100%.

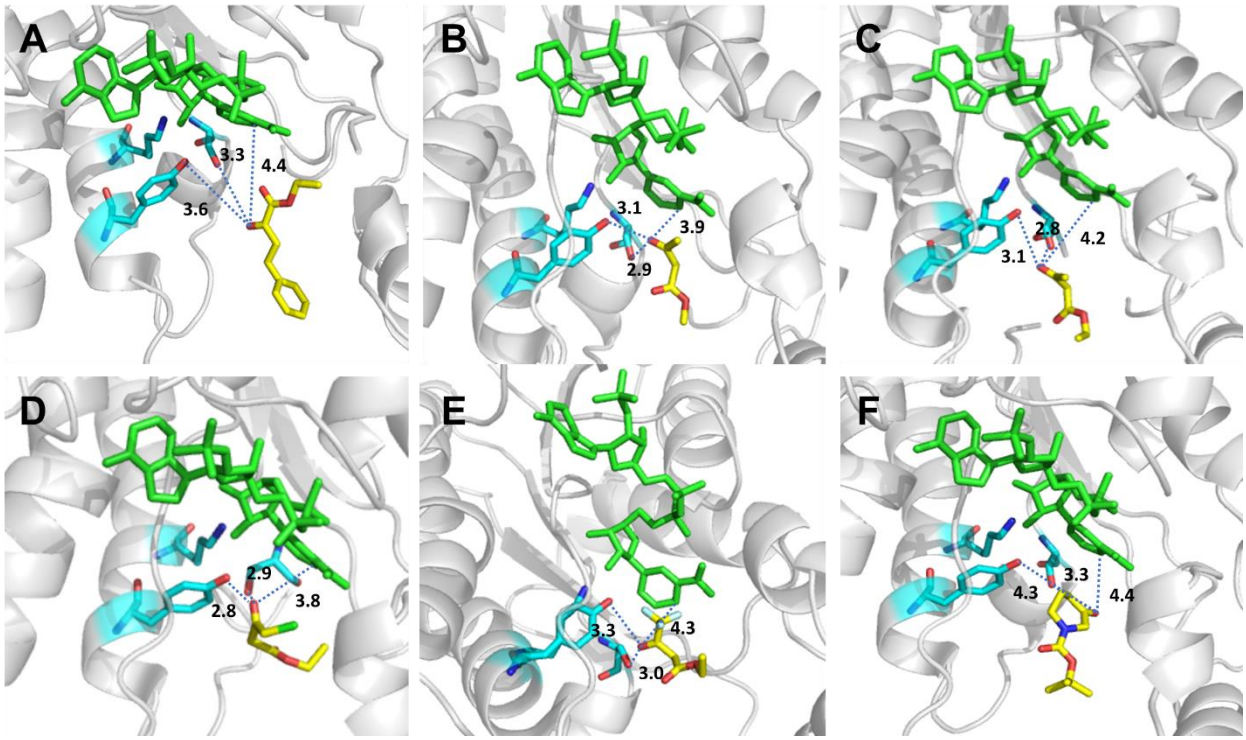

Figure S4. 3D structure generated by docking of **5a**, **6a**, **7a**, **10a**, **11a**, and **24a** into the active sites of *Sm*ADH31 and the comparison of the binding modes used for each of these substrates using MM-PB(GB) /SA. (A) **5a**; (B) **6a**; (C) **7a**; (D) **10a**; (E) **11a**; (F) **24a**. Substrate, NADPH and catalytic triads are shown as yellow sticks, green sticks and blue sticks, respectively. The distances between the substrate and the catalytic center are highlighted as blue dotted lines.

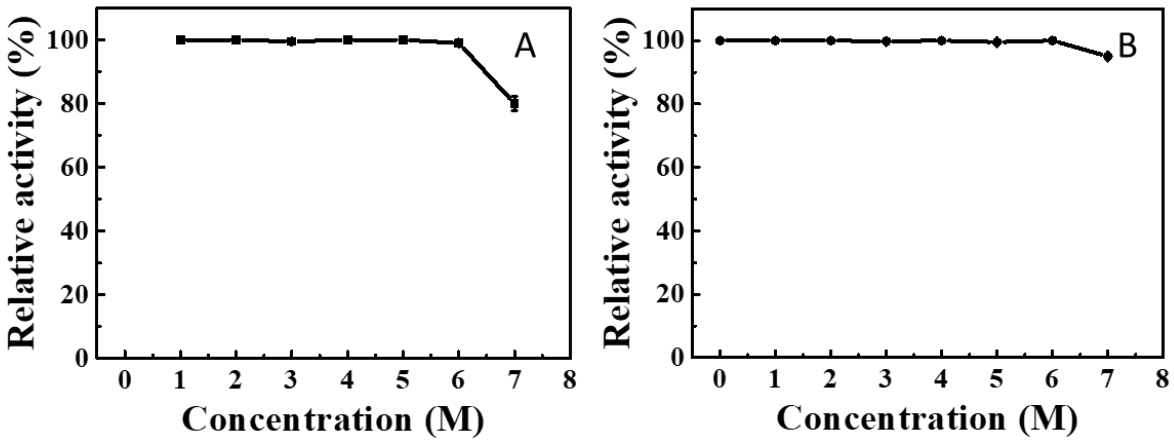

Figure S5. (A) The concentration-activity curve for the evaluation of substrate inhibition for *Sm*ADH31 at varying concentrations of COBE. (B) The concentration-activity curve for evaluating the product inhibition of *Sm*ADH31 at various (*S*)-CHBE concentration.

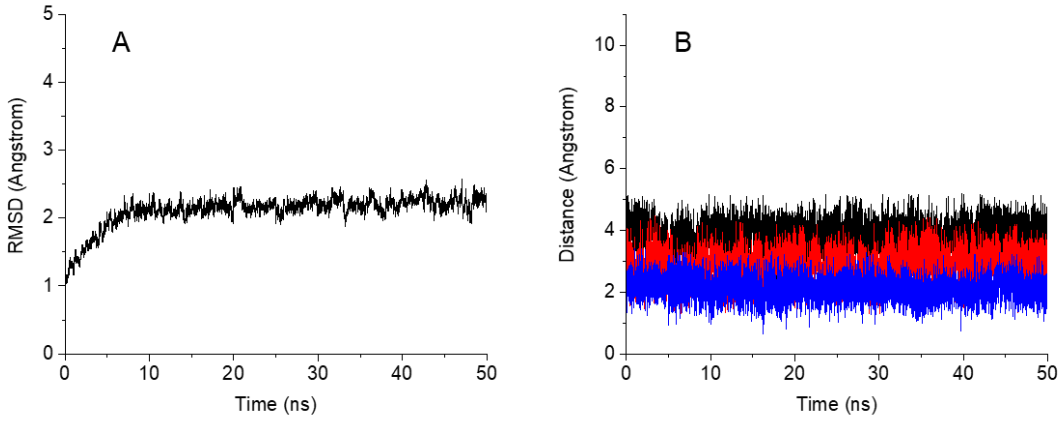

Figure S6. (A) Root-mean-square deviations analysis. (B) The distances between the carbonyl group of COBE and the hydrogen on the C4 of NADPH, Tyr152 and Ser139 are shown as black, blue and red lines.

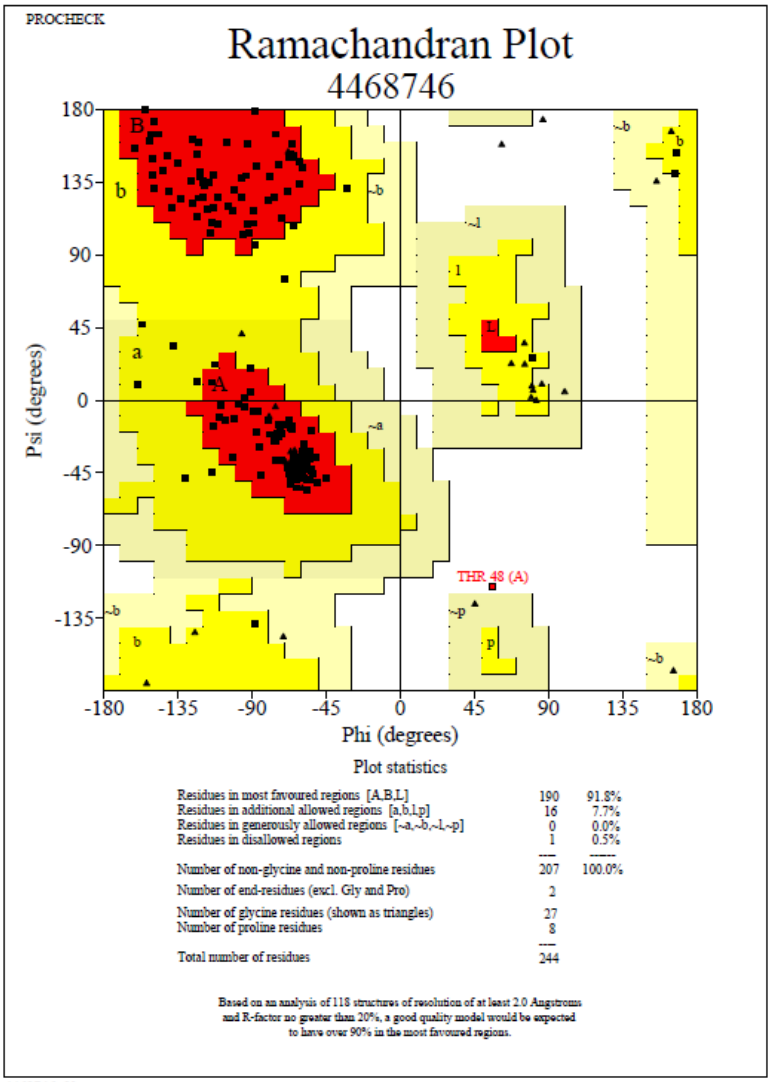

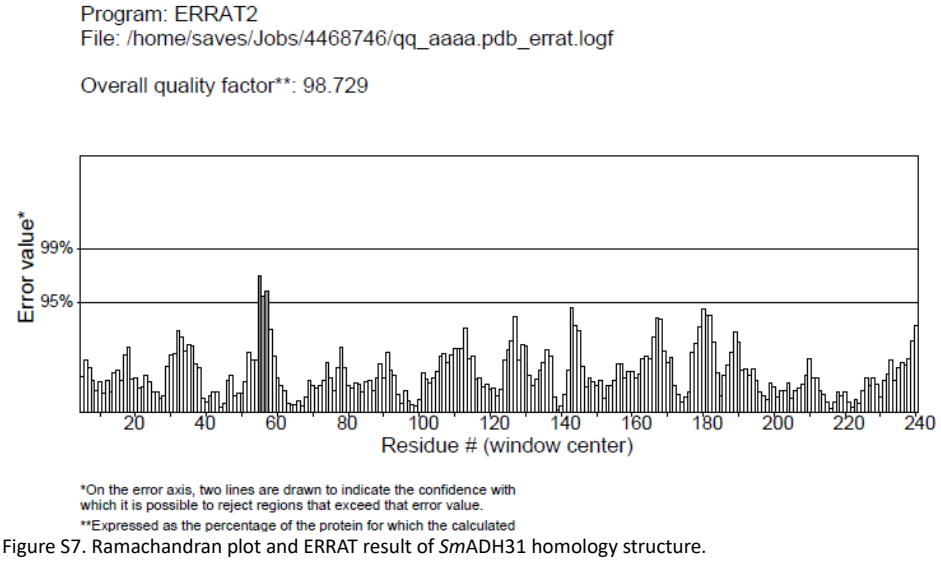

Figure S7. Ramachandran plot and ERRAT result of *Sm*ADH31 homology structure.

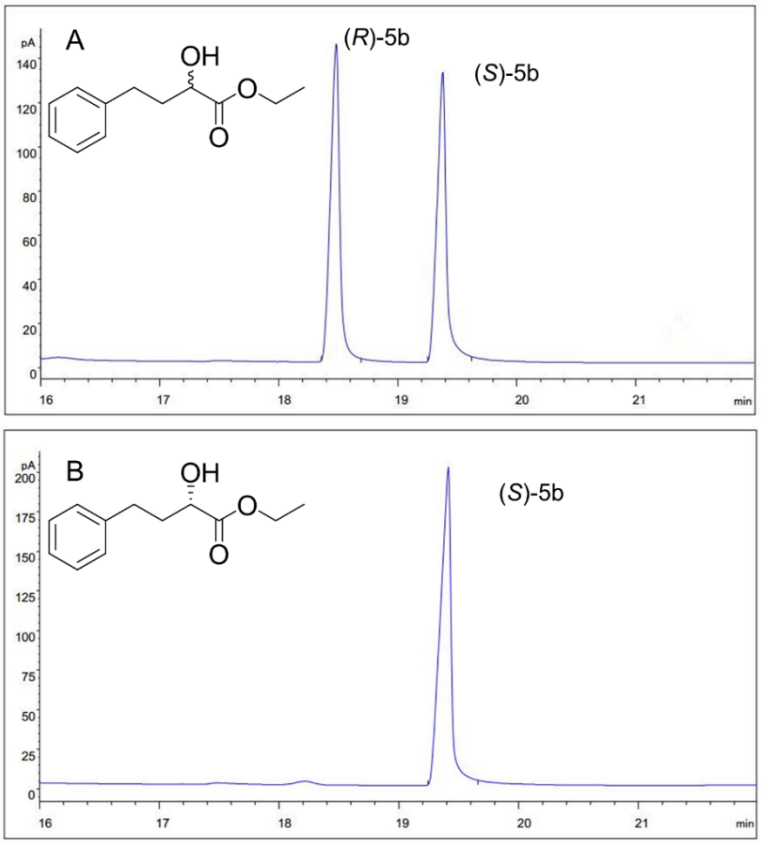

Figure S8. (A) Chiral GC analysis of (*R*)-**5b** and (*S*)-**5b**. (B) Chiral GC analysis of product **5b** produced by *Sm*ADH31.

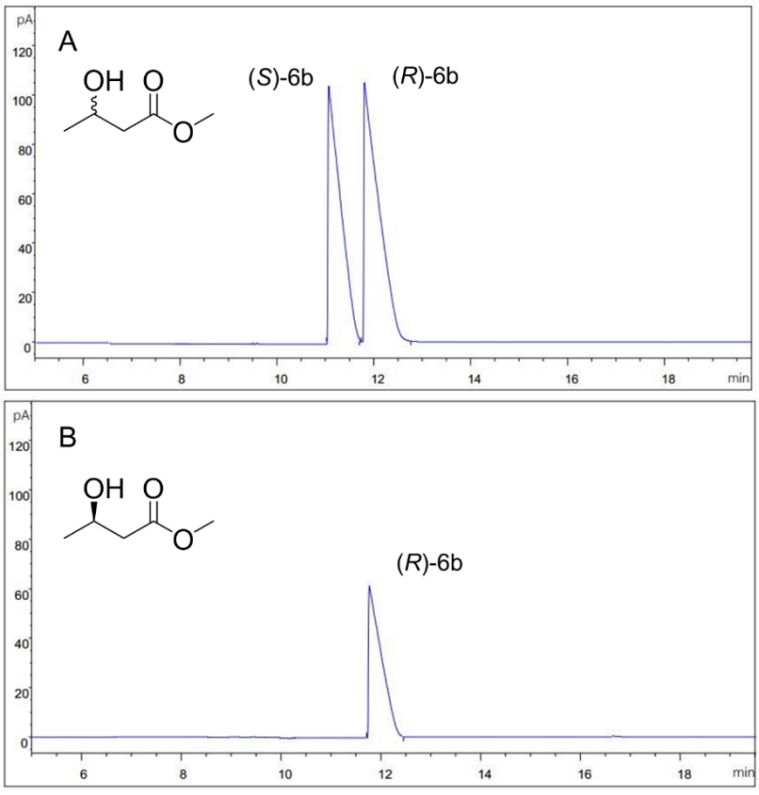

Figure S9. (A) Chiral GC analysis of (*R*)-**6b** and (*S*)-**6b**. (B) Chiral GC analysis of product **6b** produced by *Sm*ADH31.

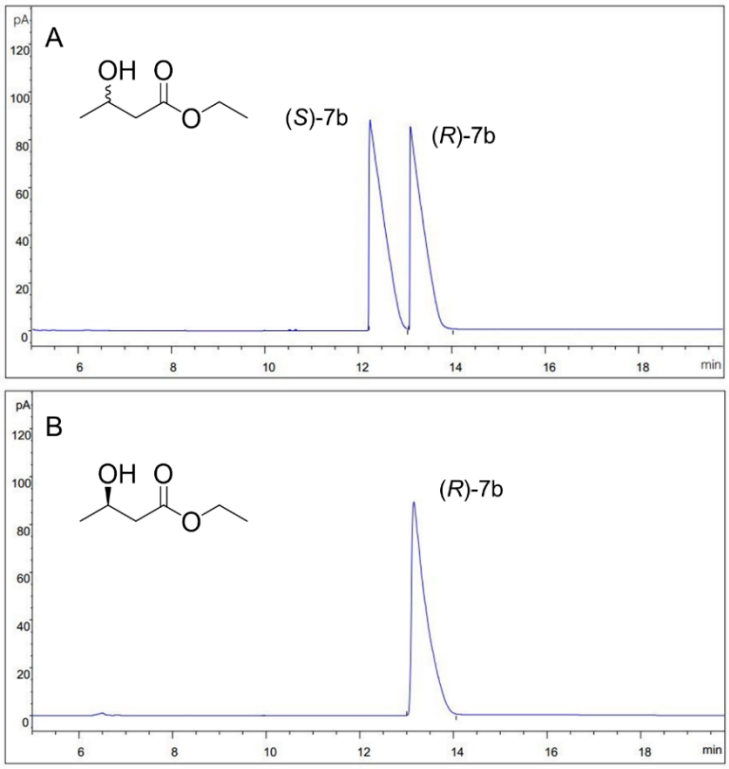

Figure S10. (A) Chiral GC analysis of (*R*)-**7b** and (*S*)-**7b**. (B) Chiral GC analysis of product **7b** produced by *Sm*ADH31.

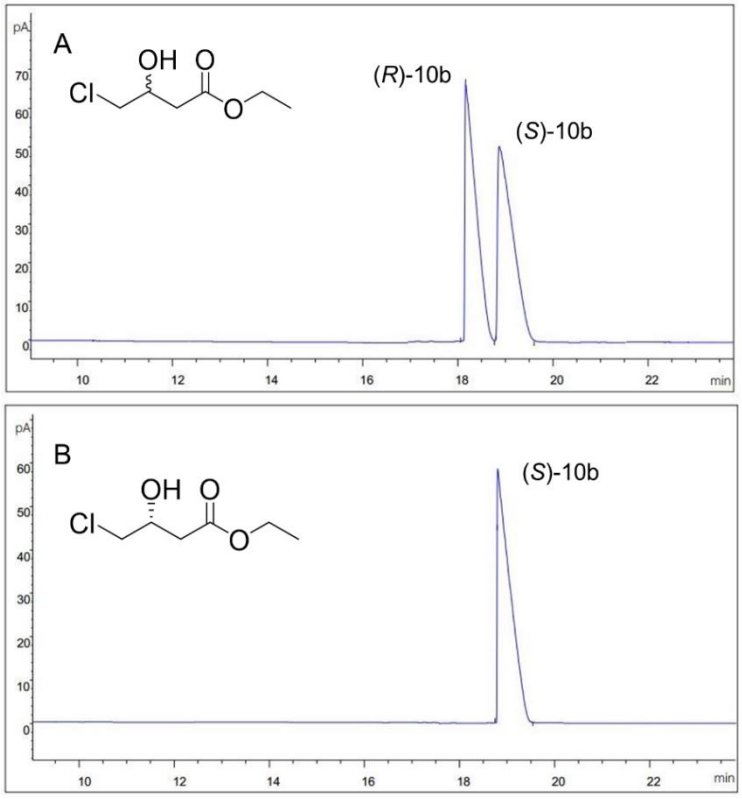

Figure S11. (A) Chiral GC analysis of (*R*)-**10b** and (*S*)-**10b**. (B) Chiral GC analysis of product **10b** produced by *Sm*ADH31.

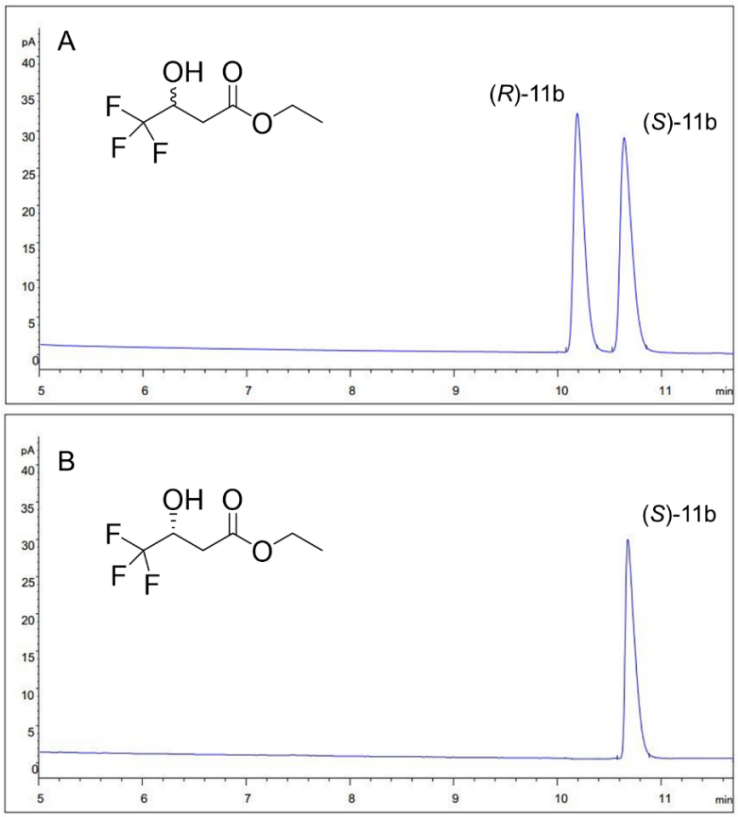

Figure S12. (A) Chiral GC analysis of (*R*)-**11b** and (*S*)-**11b**. (B) Chiral GC analysis of product **11b** produced by *Sm*ADH31.

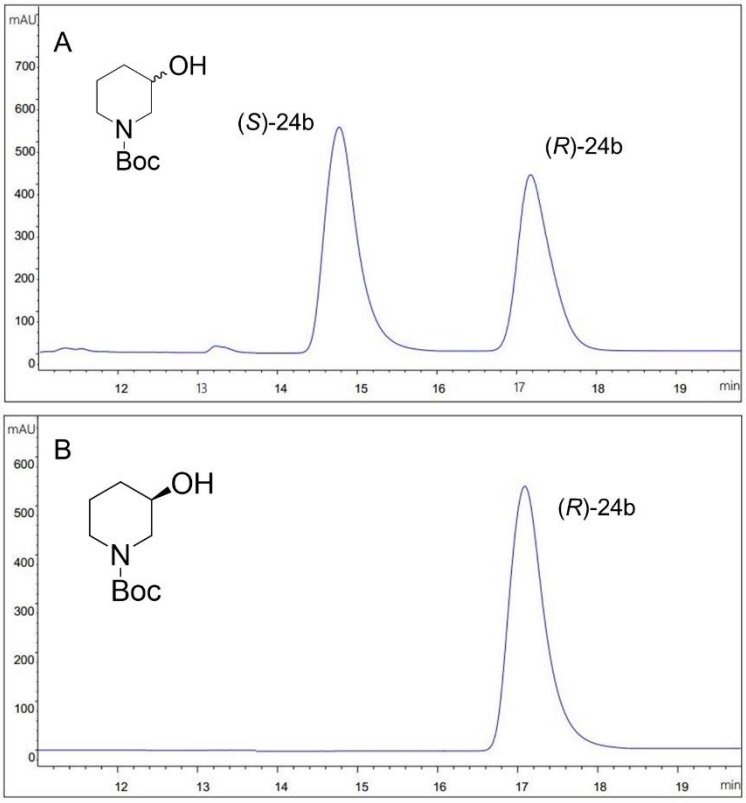

Figure S13. (A) Chiral HPLC analysis of (*R*)-**24b** and (*S*)-**24b**. (B) Chiral GC analysis of product **24b** produced by *Sm*ADH31.

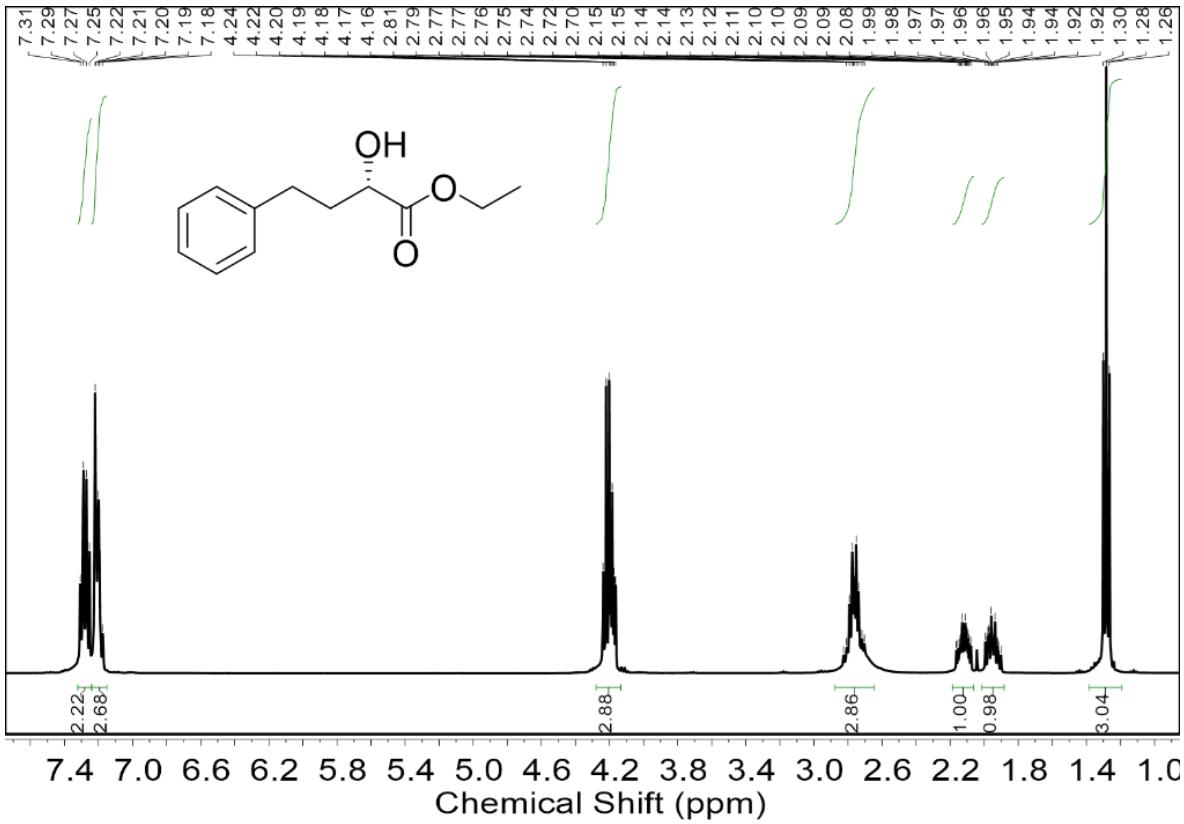

Figure S14. ^{1}H NMR spectrum of (*S*)-**5b**. ^{1}H NMR (400 MHz, Chloroform-*d*) δ 7.28 (q, *J* = 7.3 Hz, 2H), 7.21 (dd, *J* = 7.8, 2.6 Hz, 3H), 4.28 – 4.13 (m, 3H), 2.76 (dh, *J* = 19.2, 6.2, 5.8 Hz, 3H), 2.12 (dddd, *J* = 13.7, 9.6, 7.2, 4.0 Hz, 1H), 2.01 – 1.88 (m, 1H), 1.28 (t, *J* = 7.1 Hz, 3H).

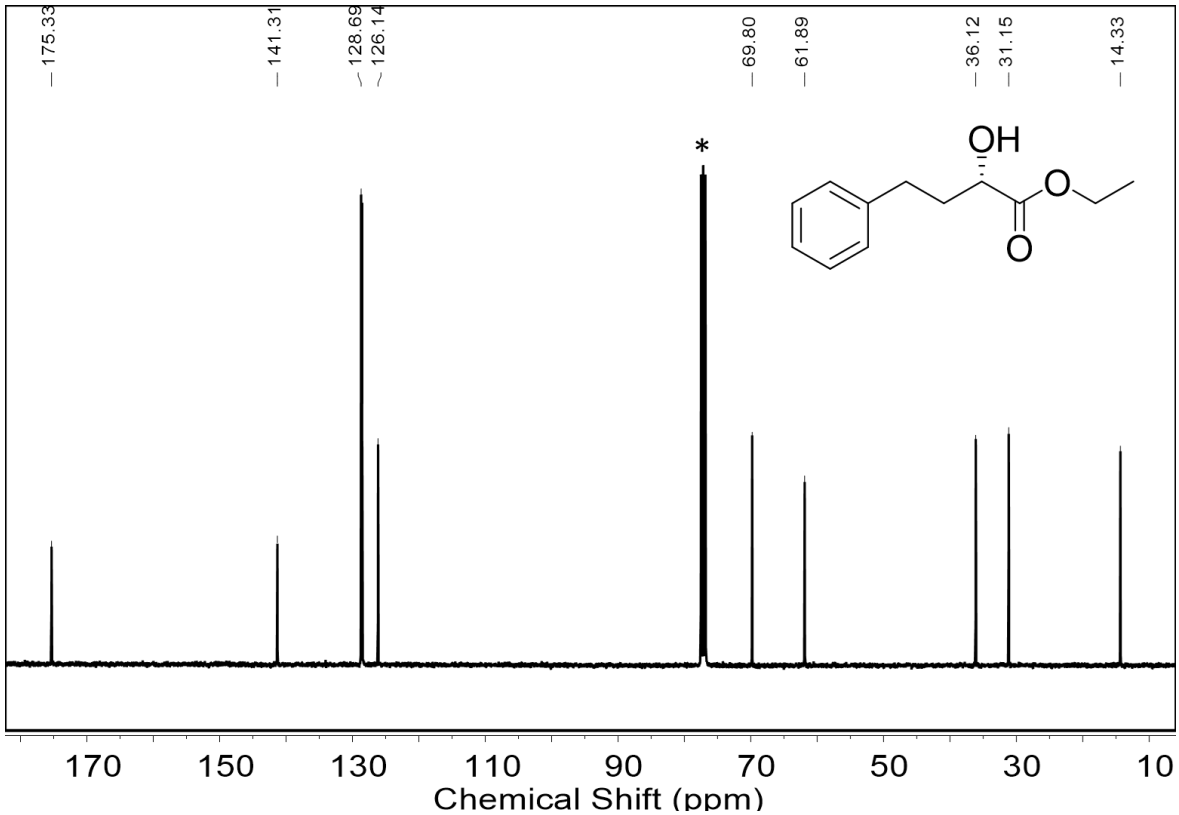

Figure S15. ^{13}C NMR spectrum of (*S*)-**5b**. ^{13}C NMR (101 MHz, Chloroform-*d*) δ 175.33 , 141.31 , 128.69 , 126.14 , 69.80 , 61.89 , 36.12 , 31.15 , 14.33 .

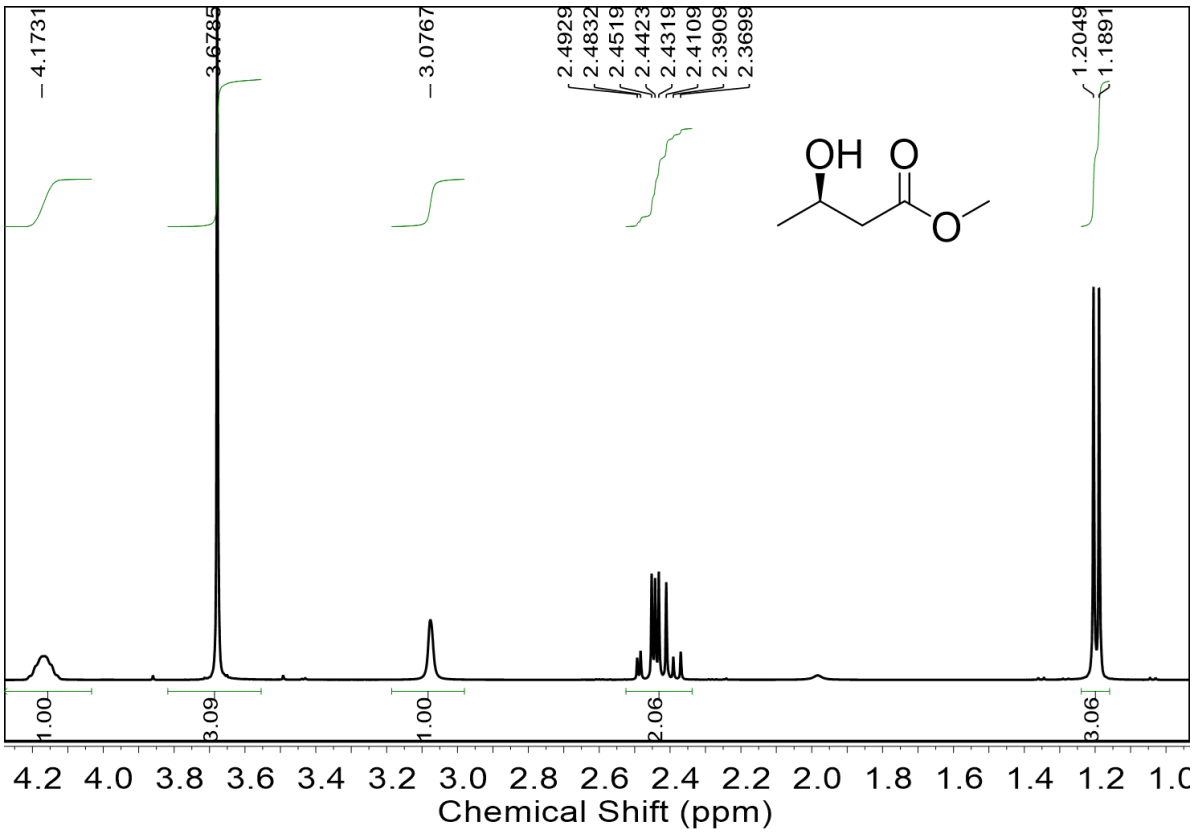

Figure S16. ^{1}H NMR spectrum of (*R*)-**6b**. ^{1}H NMR (400 MHz, Chloroform-*d*) δ 4.17 (s, 1H), 3.68 (s, 3H), 3.08 (s, 1H), 2.51 – 2.36 (m, 2H), 1.20 (d, *J* = 6.3 Hz, 3H).

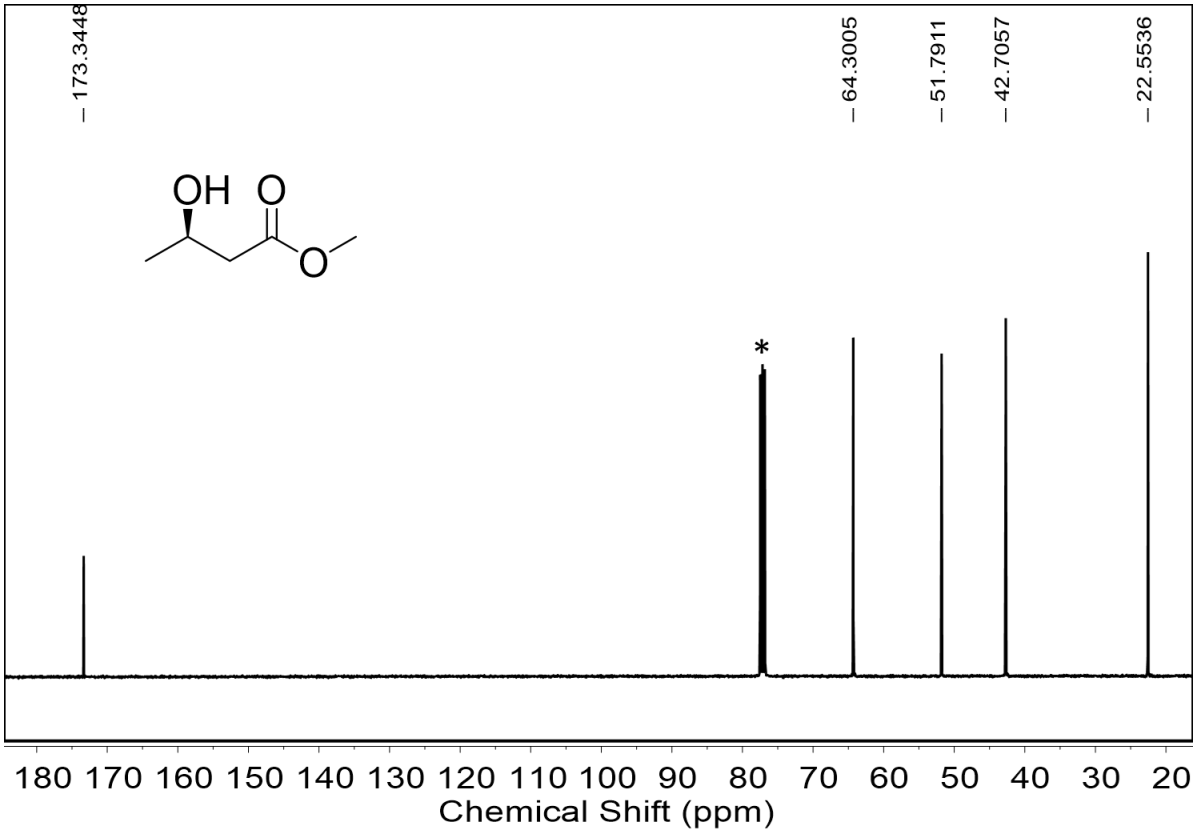

Figure S17. ^{13}C NMR spectrum of (*R*)-**6b**. ^{13}C NMR (101 MHz, Chloroform-*d*) δ 173.34 , 64.30 , 51.79 , 42.71 , 22.55 .

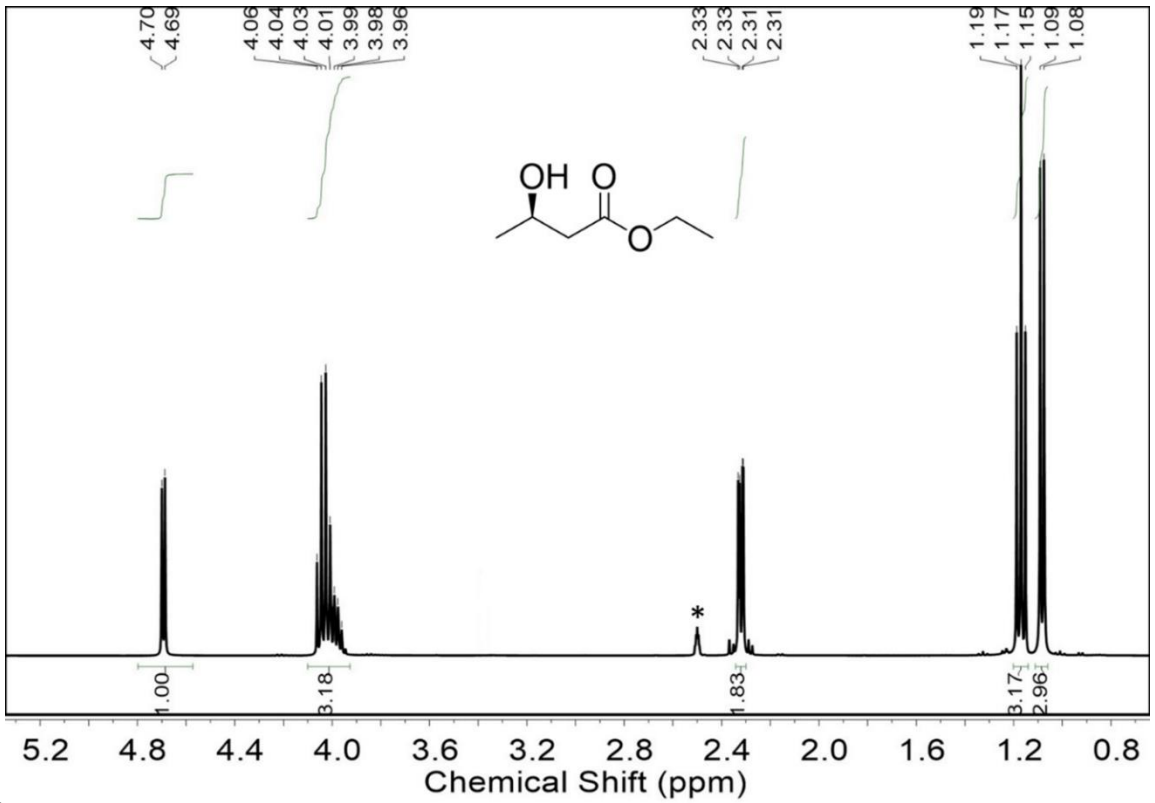

Figure S18. ^{1}H NMR spectrum of (*R*)-**7b**. ^{1}H NMR (400 MHz, DMSO-d_6) δ 4.69 (d, *J* = 5.1 Hz, 1H), 4.02 (dq, *J* = 13.1, 6.6, 6.0 Hz, 3H), 2.32 (dd, *J* = 6.6, 1.9 Hz, 2H), 1.17 (t, *J* = 7.1 Hz, 3H), 1.08 (d, *J* = 6.2 Hz, 3H). * $(CD_3)_2SO$ (2.50 ppm)

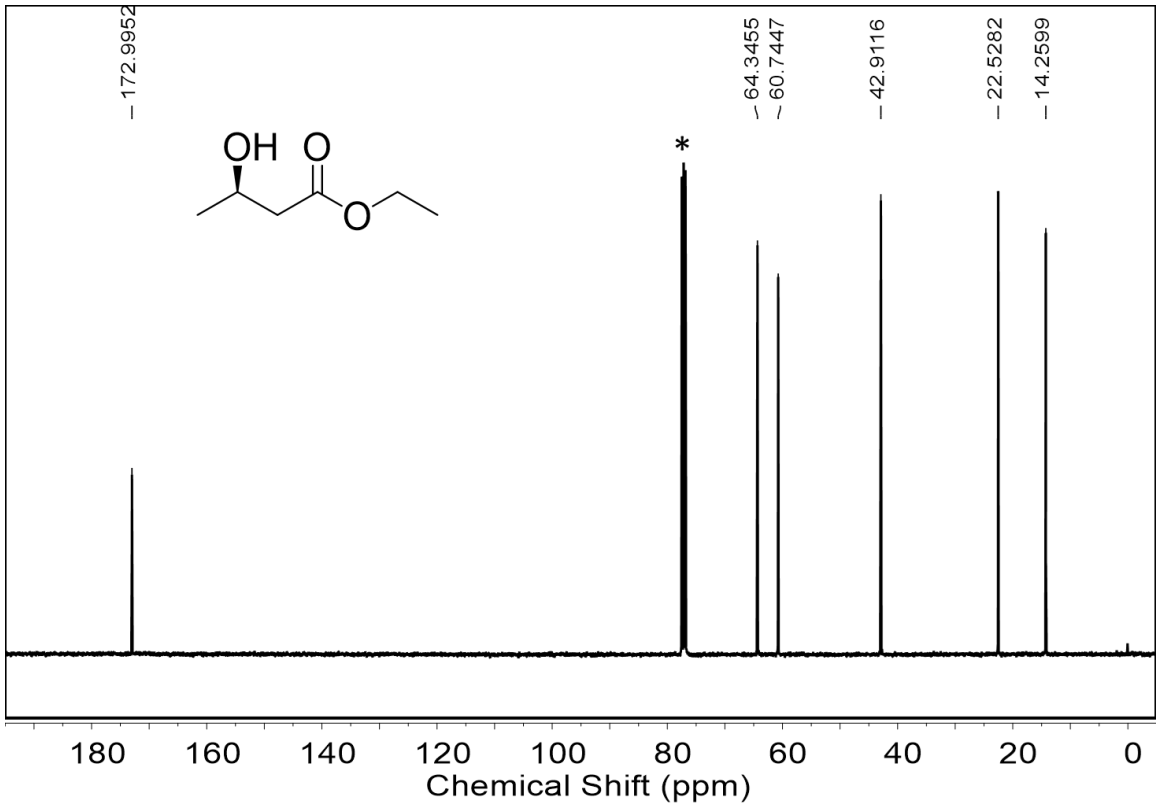

Figure S19. ^{13}C NMR spectrum of (*R*)-**7b**. ^{13}C NMR (101 MHz, Chloroform-*d*) δ 173.00 , 64.35 , 60.74 , 42.91 , 22.53 , 14.26 .

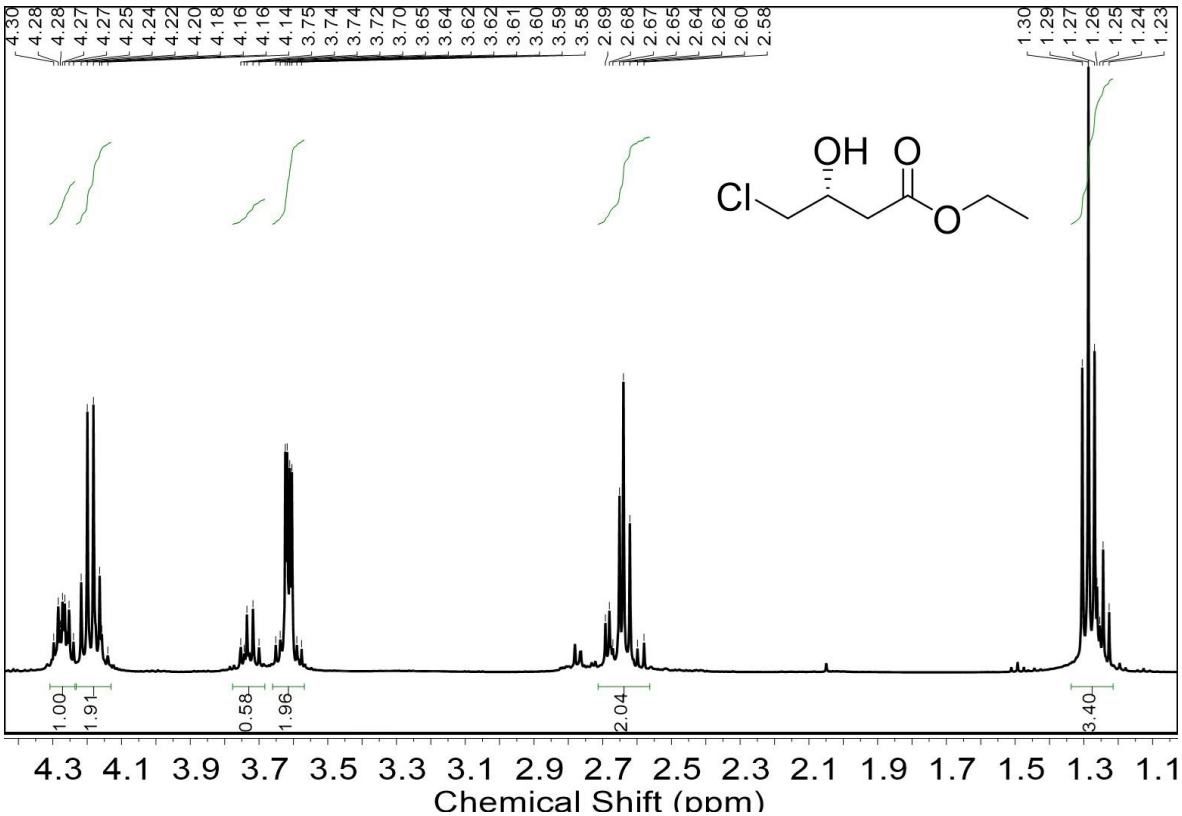

Figure S20. ^{1}H NMR spectrum of (*S*)-**10b**. ^{1}H NMR (400 MHz, Chloroform-*d*) δ 4.31 – 4.24 (m, 1H), 4.19 (q, *J* = 7.1 Hz, 2H), 3.73 (q, *J* = 7.1 Hz, 1H), 3.66 – 3.57 (m, 2H), 2.71 – 2.56 (m, 2H), 1.27 (dt, *J* = 17.0, 7.1 Hz, 3H).

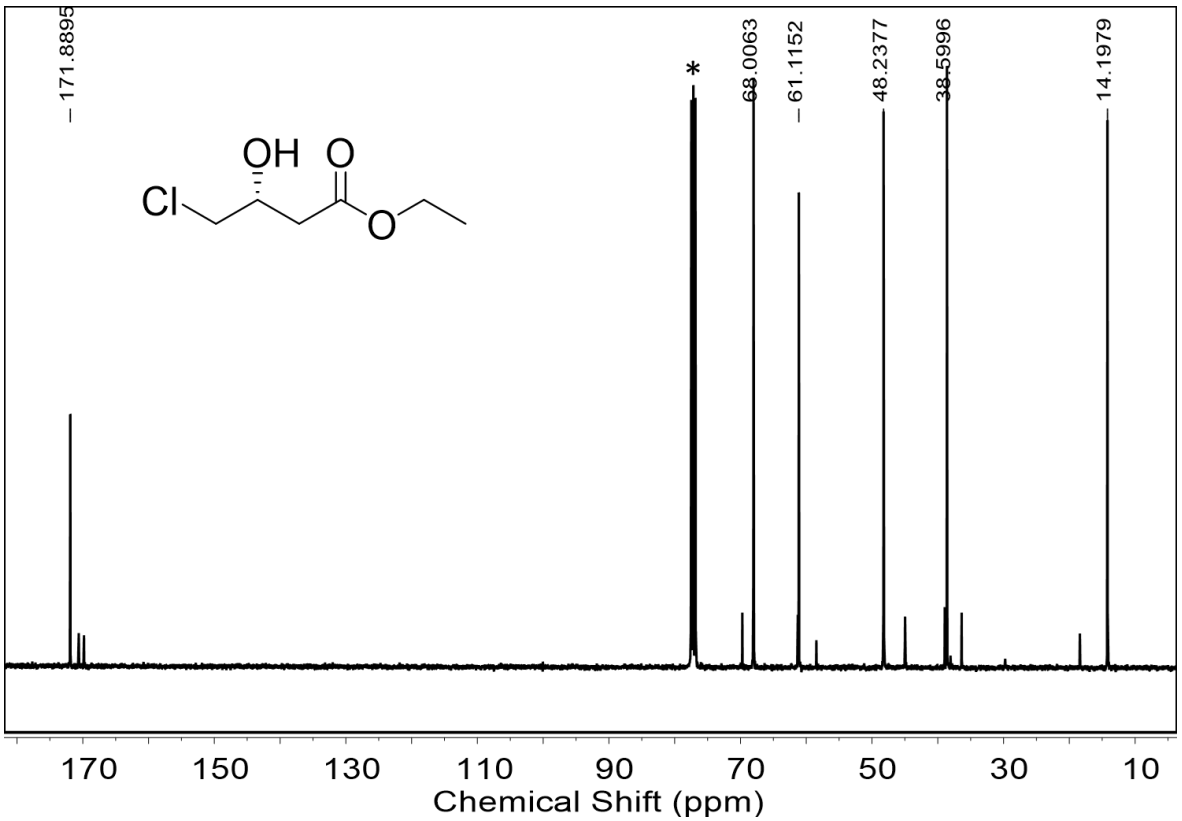

Figure S21. ^{13}C NMR spectrum of (*S*)-**10b**. ^{13}C NMR (101 MHz, Chloroform-*d*) δ 171.89 , 68.01 , 61.12 , 48.24 , 38.60 , 14.20 .

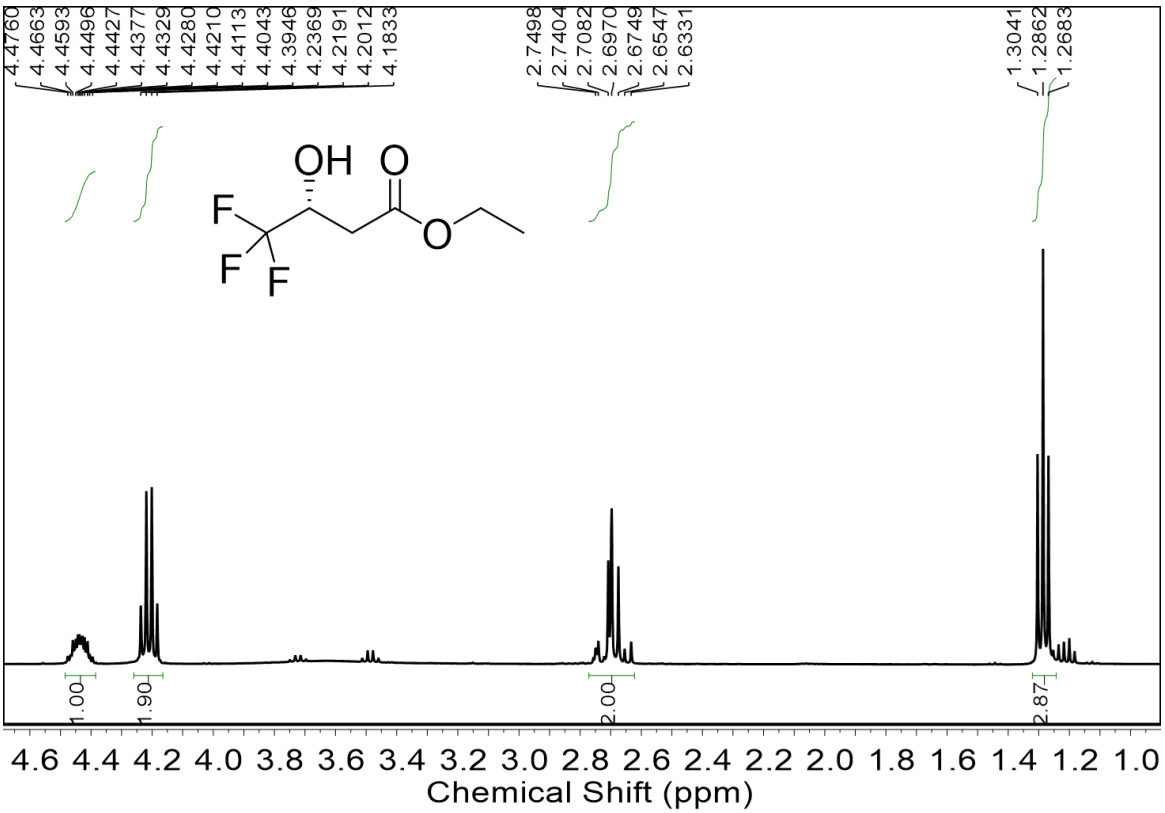

Figure S22. ^{1}H NMR spectrum of (*S*)-**11b**. ^{1}H NMR (400 MHz, Chloroform-*d*) δ 4.44 (ddq, *J* = 11.4, 6.7, 2.8 Hz, 1H), 4.21 (q, *J* = 7.1 Hz, 2H), 2.77 – 2.62 (m, 2H), 1.29 (t, *J* = 7.2 Hz, 3H).

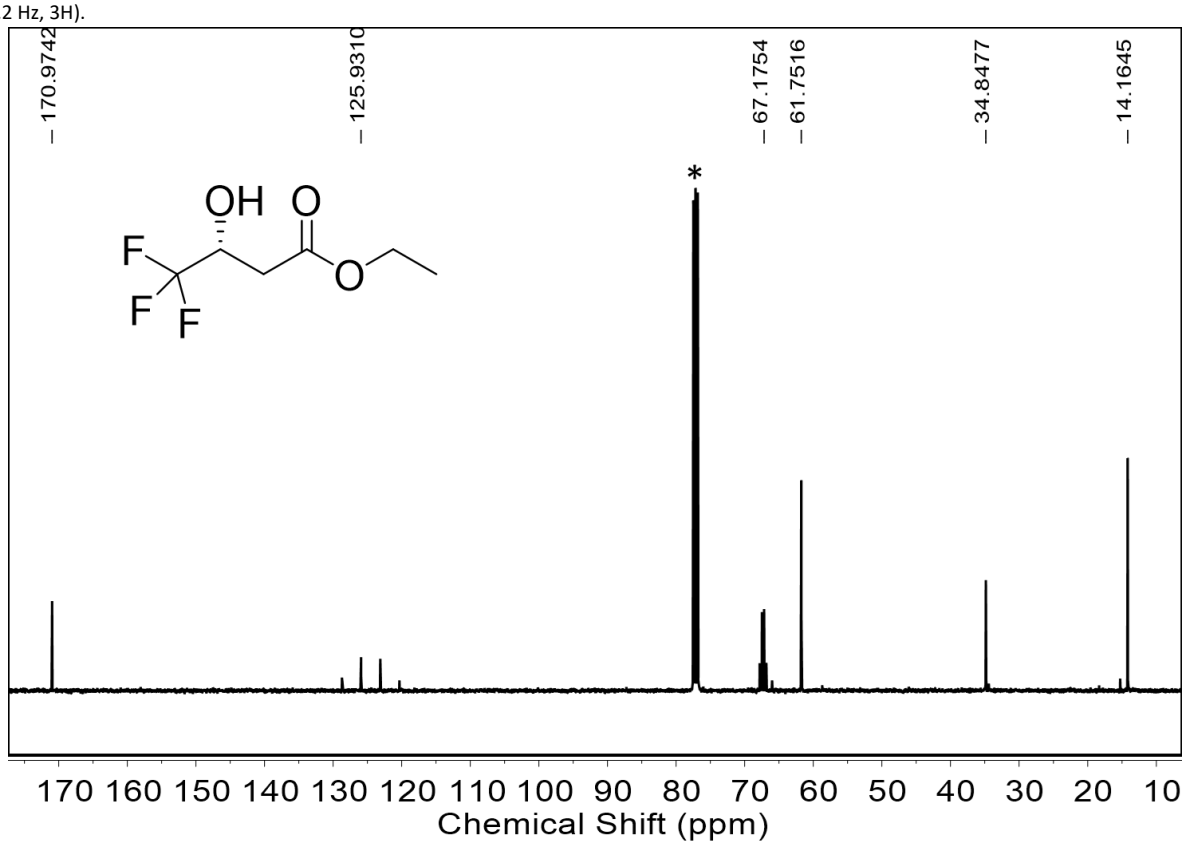

Figure S23. ^{13}C NMR spectrum of (*S*)-**11b**. ^{13}C NMR (101 MHz, Chloroform-*d*) δ 170.97 , 125.93 , 67.18 , 61.75 , 34.85 , 14.16 .

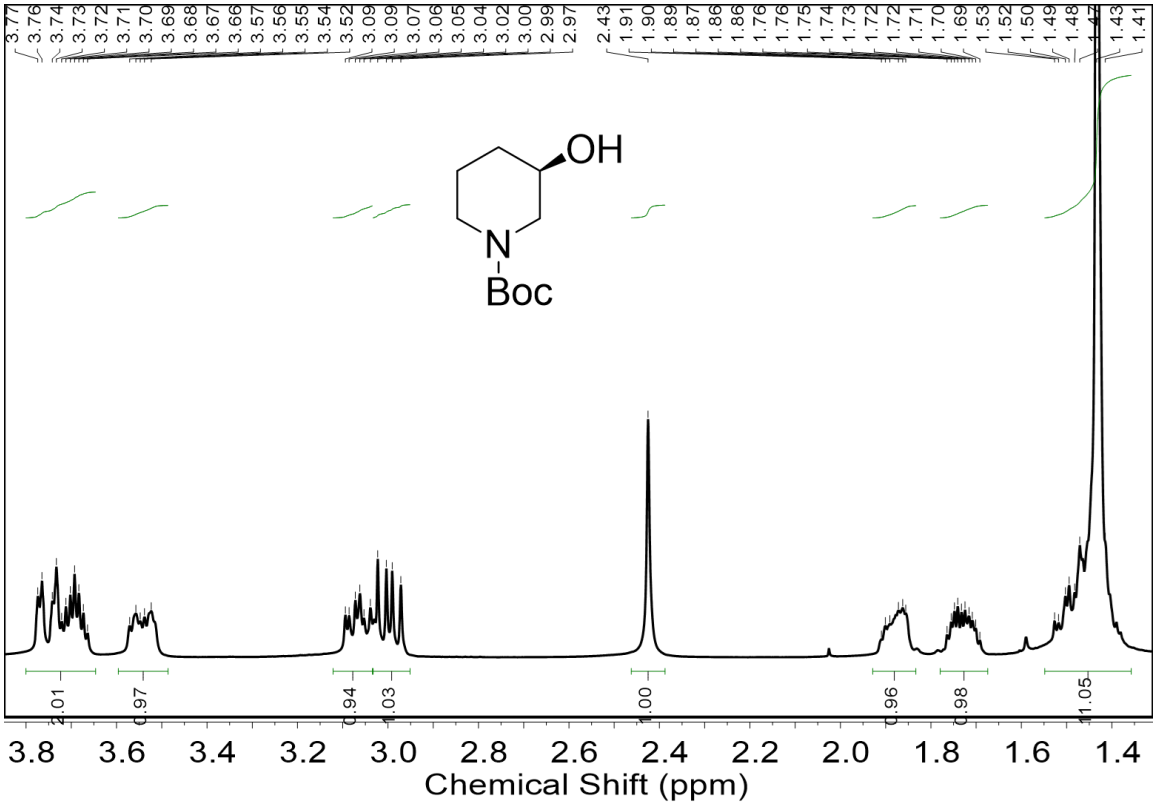

Figure S24. ^{1}H NMR spectrum of (*R*)-**24b**. ^{1}H NMR (400 MHz, Chloroform-*d*) δ 3.80 – 3.65 (m, 2H), 3.60 – 3.49 (m, 1H), 3.07 (td, *J* = 9.1, 4.5 Hz, 1H), 3.00 (dd, *J* = 12.8, 7.6 Hz, 1H), 2.43 (s, 1H), 1.93 – 1.83 (m, 1H), 1.73 (ddq, *J* = 13.1, 6.7, 3.6 Hz, 1H), 1.43 (s, 11H).

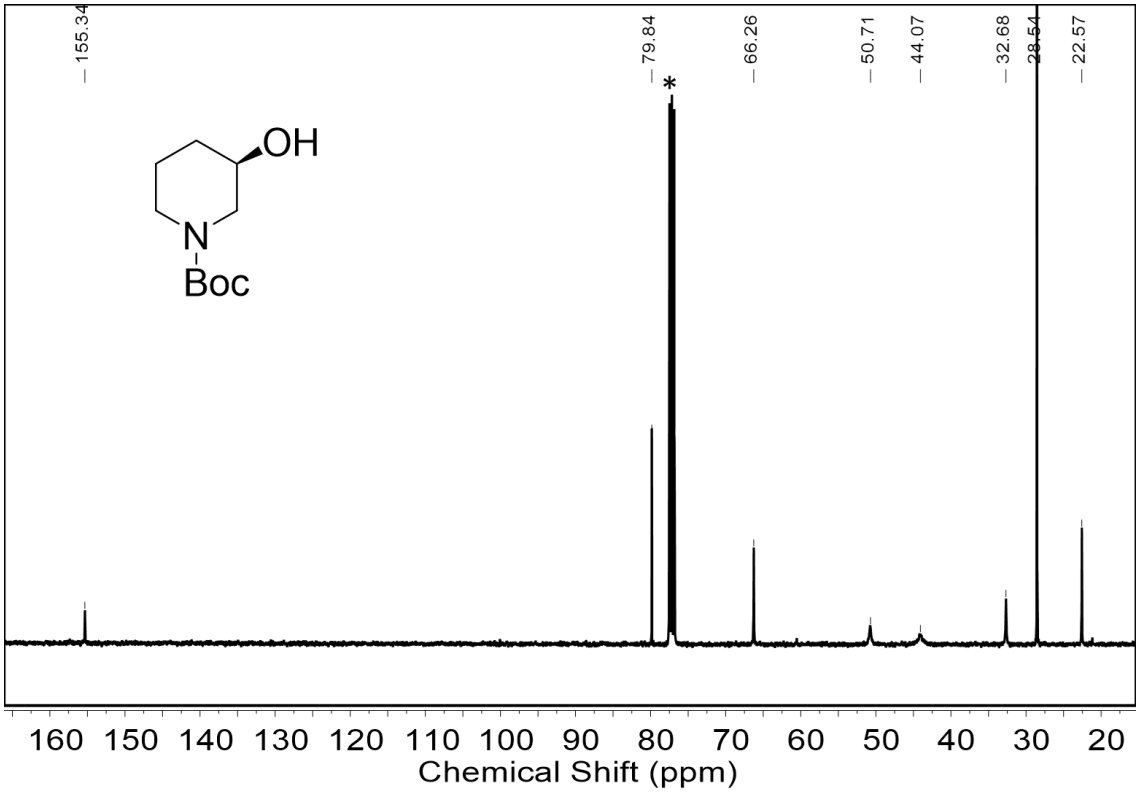

Figure S25. ^{13}C NMR spectrum of (*R*)-**24b**. ^{13}C NMR (101 MHz, Chloroform-*d*) δ 155.34 , 79.84 , 66.26 , 50.71 , 32.68 , 28.54 , 22.57 .

References:

1. Yang, Z. Y.; Fu, H. W.; Ye, W. J.; Xie, Y. Y.; Liu, Q. H.; Wang, H. L.; Wei, D. Z. Efficient asymmetric synthesis of chiral alcohols using high 2-propanol tolerance alcohol dehydrogenase *Sm*ADH2 via an environmentally friendly TBCR system, *Catal. Sci. Technol.* **2020,** *10*, 70-78.